



# Creep characteristics and prediction of creep failure of rock discontinuities under shearing conditions

Zhen Wang<sup>1,3</sup> · Linlin Gu<sup>2</sup> · Qingzhao Zhang<sup>4,5</sup> · Songlin Yue<sup>3</sup> · Guokai Zhang<sup>1</sup>

Received: 4 December 2019 / Accepted: 24 February 2020 / Published online: 12 March 2020  
© Geologische Vereinigung e.V. (GV) 2020

## Abstract

Shear creep is one of the most important mechanical behaviors of rock discontinuities. The creep mechanism and prediction of starting point of the accelerating creep stage are vital for establishing the creep model and predicting creep failure. In this study, a series of multi-step creep tests are conducted. The three creep stages of shear creep tests are investigated in detail, and a method for predicting the accelerating creep stage is proposed. Distinct nonlinear and local fluctuations caused by cracking are observed in the creep curve. To describe the transition creep stage and steady creep stage, an empirical creep model is established, and the creep characteristics related to the joint roughness coefficient (JRC) and the normal stress are explored in detail using the model's parameters. The creep process can be described as involving the JRC resistance weakening and frictional resistance compensation, and a model also established to describe this process. The frictional resistance cannot compensate for the loss of JRC resistance; consequently, creep failure occurs. The starting point of the accelerating creep stage can be predicted by combining the JRC weakening and frictional mobilization model and the empirical creep model. A new method for determining long-term strength is also proposed based on the relationships between the starting point creep deformation and the shear creep stress.

**Keywords** Creep · Rock discontinuity · Creep model · Accelerating creep stage

---

**Electronic supplementary material** The online version of this article (<https://doi.org/10.1007/s00531-020-01842-8>) contains supplementary material, which is available to authorized users.

---

✉ Linlin Gu  
linlin\_gu@njjust.edu.cn

<sup>1</sup> School of Mechanical Engineering, Nanjing University of Science and Technology, Nanjing 210094, China

<sup>2</sup> Department of Civil Engineering, Nanjing University of Science and Technology, Nanjing 210094, China

<sup>3</sup> State Key Laboratory of Disaster Prevention and Mitigation of Explosion and Impact, The Army Engineering University of PLA, Nanjing 210014, China

<sup>4</sup> Key Laboratory of Geotechnical and Underground Engineering of Ministry of Education, Tongji University, Shanghai 200092, China

<sup>5</sup> Department of Geotechnical Engineering, Tongji University, Shanghai 200092, China

## Introduction

Discontinuities, such as bedding planes, faults, and joints, considerably influence the mechanical characteristics of rock mass (Mulchrone and Mukherjee 2015) and even control the stability of rock mass. The sliding of rock discontinuities can lead to earthquake, landslide, and other related disasters (Oppikofer 2009; Araki 2017). The creep behavior of rock discontinuity significantly influences the long-term stability. Rock discontinuity can deform nonlinearly over an extended period of time and fail or slip under creep stress below the short-term failure strength (Heap et al. 2009a). In this process, accelerating deformation precedes creep deformation accumulated and macroscopic failure (Brantut et al. 2012, 2013).

Considerable efforts have been made over the past few years to investigate and understand creep of rock discontinuity (Drescher and Handley 2003; Asanov and Pan'Kov 2004; Zhang et al. 2011; Wang et al. 2018). Drescher and Handley (2003) conducted shear creep tests on artificial joint surfaces with discontinuity infillings (crushed lava, crushed quartzite, and natural gouge) at various shear stress levels

from 60% of expected failure load to failure stress, incremented by 5% of expected failure load. Asanov and Pan'Kov (2004) performed the shear creep tests with different normal stress on the rock discontinuity. They observed three typical creep stages: transition creep stage, steady creep stage, and accelerating creep stage. The creep rate depends on the shear stress to shear strength ratio (Drescher and Handley 2003; Wang et al. 2018). Zhang et al. (2011) tested the mechanical behavior of white marbles with weak structural planes using the multi-stage loading shear creep method. They found that the weak structural planes of greenschist distinctly exhibited brittle failure characteristics, and the shear creep test curve of the structural plane also exhibited three distinct stages. The results indicate that the creep characteristics, including creep rate, creep deformation, and creep stages, resemble those of the creep tests of intact samples. The creep behavior of rock discontinuities, however, remains to have a certain particularity because of the complex surface morphology of rock discontinuity. Rock discontinuity's roughness and its occurrence influenced the creep deformation, creep strength, and even creep failure mode (Wang et al. 2017). It has been found that creep deformation increased with the increase in joint roughness, and the creep behavior of rock discontinuity is considerably influenced by the surface morphology (Wang et al. 2018). However, the investigations related to the shear creep testing of rock discontinuities under constant shear stress loading are limited, especially at accelerating creep stage.

The creep model is one of the key aspects involved in the investigation of creep characteristics. In recent years, certain creep models, such as the empirical creep model (Singh 1975), element model (Sakurai 1978; Boidy et al. 2002; Zhu et al. 2009; He et al. 2014), damage fracture model (Kemeny 2003, 2005), and viscoelastic–plastic model (Zhang et al. 2019), have been proposed. For example, Potyondy and Cundall (2004, 2007) proposed a bond-particle model to simulate the stress-corrosion process which is the primary mechanism of the time-dependent behavior of rock in the brittle regime. Kemeny (2003, 2005) proposed a fracture mechanics model to simulate the time-dependent failure of rock bridges along discontinuities. The element model was very popular in the research of creep model (Phienweij et al. 2007). Zhu et al. (2009) performed a back analysis of model parameters using six general shear creep models, but the parameters are all regarded to be stationary. In reality, however, as creep progresses, its parameters are usually non-stationary (Xu et al. 2013). He et al. (2014) proposed a generalized Kelvin model to describe both the transition and steady creep stages. They also established a non-linear creep damage model based on the creep damage characteristics to describe the accelerating creep stage. Most creep models with a superposition of a small number of viscous and elastic elements, however, cannot explain the accelerating

creep stage. To describe the abovementioned stage, more complex models with an extremely large number of elastic and viscous elements are necessary; however, because the parameters are overly numerous, their physical meanings are unclear (Xu et al. 2013).

The piecewise function is often used in the creep model, but the starting point of the accelerating creep stage is difficult to identify. The threshold for judging whether an accelerated creep stage occurs in the creep tests remains to be the long-term strength that is difficult to determine. Besides, the long-term strength can just be used to predict whether the creep will enter the accelerating creep stage. However, it cannot be used to determine under what conditions or at what time the creep enters the accelerated creep stage, thereby making it difficult to predict the delayed sliding and related disasters. Therefore, although certain progress has been made in recent years, some problems necessitate further research.

In this study, multi-step creep tests are conducted on artificial rock discontinuities, and the characteristics and creep mechanism of the three creep stages are investigated in detail. A creep model named Joint roughness (described by JRC) resistance weakening and frictional resistance compensation creep model (JRCWC model) that uses the concept of JRC resistance weakening and frictional compensation is established. A method for predicting the starting point of the accelerating creep stage based on the JRCWC model and empirical creep model is proposed. The starting point characteristics are further explored accordingly, and a new method for determining the long-term strength is also proposed.

## Methodology

### Testing equipment

In this study, the shear tests and shear creep tests are performed using a servo-controlled rheological testing device (CSS-1950), as shown in Fig. 1. The maximum compression loads in the vertical and horizontal directions are 500 and 300 kN, respectively. The stress can be maintained constant for more than 500 h with errors < 1 N. The vertical and horizontal deformations are measured via two linear variable displacement transducers. The accuracy rate of deformation measurement is 1  $\mu\text{m}$  in the range 0–10 mm.

### Sample

The artificial sample made of cement-mortar is widely used to simulate rock mass because of its homogeneity and rock-like properties. A large number of experimental results have been obtained using cement-mortar artificial rock



Fig. 1 CSS-1950 servo-controlled rheological testing machine

discontinuities, and a significant time-dependent behavior has been observed through creep, stress relaxation, and shear rate-dependent behavior tests (Patton et al. 1966; Einstein

et al. 1983; Wang et al. 2018, 2020). In the creep tests, the weight ratio of water, cement, and sand is 1:2:4. The physical–mechanical property parameters of cement-mortar based on physical, uniaxial, and triaxial compression tests in accordance with the International Society for Rock Mechanics are listed in Table 1 (Ulusay 2015).

The production process of samples that is similar to that employed in the research of Wang et al. (2019) is shown in Fig. 2. The samples are prepared with cement-mortar using a steel mold that is fabricated based on Barton’s standard profiles (Barton and Choubey 1978). The cement-mortar is well-mixed before it is poured into the steel mold. The samples are shaken for 1 h and removed from the mold 24 h later. The samples are thereafter stored in a curing room for 28 days. The temperature and humidity of the curing room are approximately  $20 \pm 1 \text{ }^\circ\text{C}$  and 95%, respectively. Each sample must be of the same mix proportion and prepared following the same procedure. The samples with different JRCs are cubic-shaped with dimensions of 10 cm (L)  $\times$  10 cm (W)  $\times$  10 cm (H), as shown in Fig. 2. Shear tests are conducted on artificial samples with different joint roughness coefficients. As summarized in

Table 1 Physical–mechanical properties of cement-mortar

Density	Void ratio/ $\rho$	Uniaxial compression strength/ $\sigma$	Cohesion/ $c$	Friction angle/ $\varphi$	Elastic Modulus/ ed	Poisson’s ratio/ $\mu$
$\text{g/cm}^3$		MPa	MPa	$^\circ$	GPa	
2.05	0.2	21.73	4.05	49.23	7.9	0.23

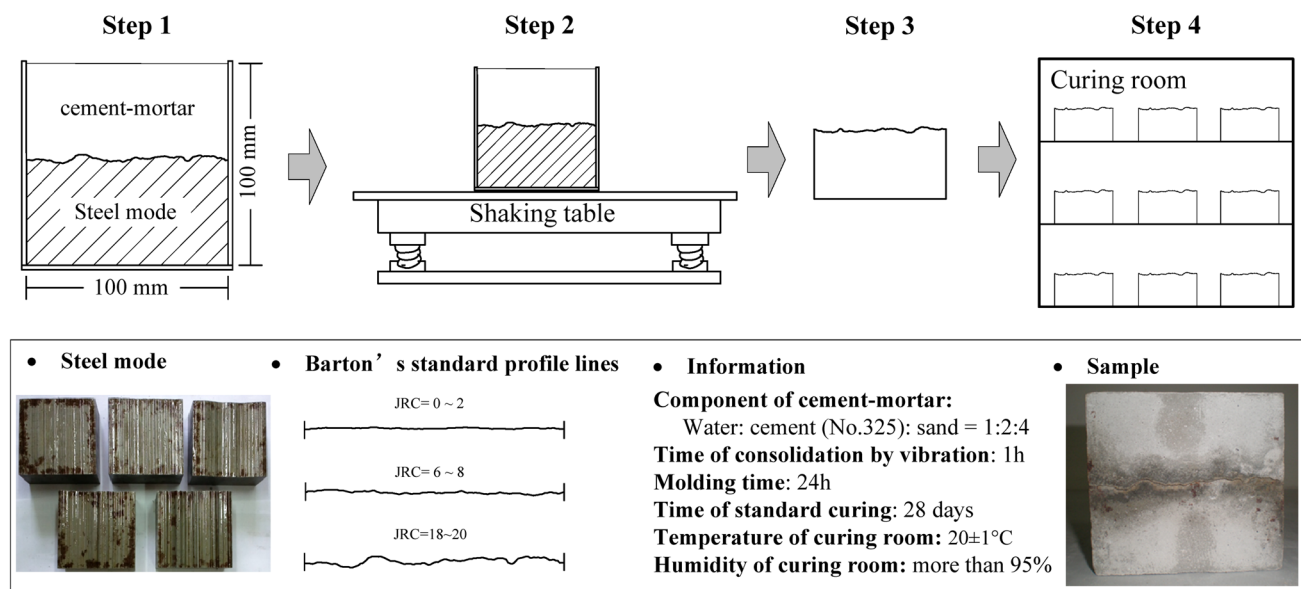
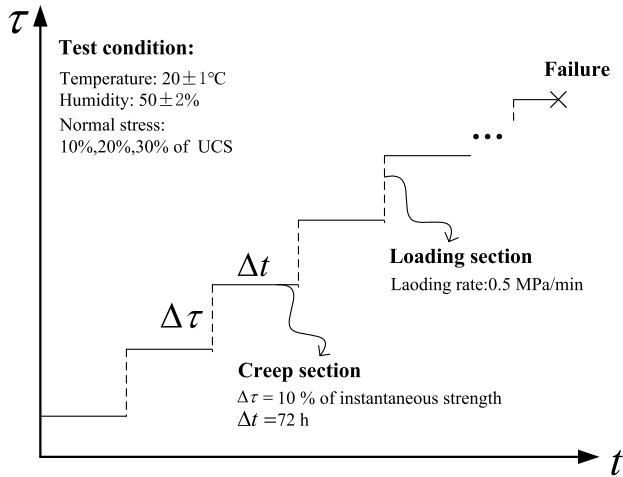


Fig. 2 Sample preparation process (Wang et al. 2020) (Step1: Put the cement-mortar into steel mold, Step 2: Shake for 1 h on the shaking table, Step 3: Remove the sample from the mold 24 h later, Step 4:

Keep the sample in curing room for 28 days. The steel mode, profile lines used in this paper, the sample preparation information, and a sample are listed in this figure)

**Table 2** Shear strength parameters of the artificial rock discontinuities

Normal stress, $\sigma_n$ /MPa	Shear strength, $\tau$ /MPa				
	JRC=0	JRC=1	JRC=7	JRC=11	JRC=19
2.17	1.36	1.76	2.2	2.71	3.58
4.35	3.84	3.89	4.54	5.15	6.25
6.52	4.41	4.70	5.31	7.19	7.9
c/MPa	0.42	0.55	0.61	0.89	1.13
$\phi/^\circ$	32.38	34.04	37.05	41.41	47.08



**Fig. 3** Shear stress path of multi-step creep tests ( $t$  time,  $\tau$  creep stress)

Table 2, the shear strength, frictional angle, and cohesion increase as the normal stress and joint roughness coefficients increase. The shear strength is used to determine the creep stresses in the multi-step creep tests, and the shear strength parameters and shear deformation curves can be used to determine the parameters of the JRC weakening and cohesion mobilization (JRCW) model (Wang et al. 2020).

### Procedure of multi-step shear creep tests

The multi-step loading method, recommended by Tan (1966) and Tan and Kang (1980), is used for the shear creep tests. The creep curves under different creep stresses that correspond to each stress step in the multi-step loading can be satisfactorily obtained from only one sample based on the general Boltzmann superposition principle (Christensen 1982). As shown in Fig. 3, the samples with the first (JRC = 1) and tenth (JRC = 19) profile lines are chosen for the multi-step shear creep tests since the large difference of the roughness would lead to the obvious test phenomenon. The normal stress of the shear creep tests is first loaded to 10% (2.17 MPa), followed by 20% (4.35 MPa) and 30% (6.52 MPa) of the unconfined compression strength, and thereafter kept constant. When the normal stress and normal deformation are stable, the shear stress is applied at a constant rate of 0.5 MPa/min. The shear stress levels are determined as 50%, 60%, 70%, 80%, and 90% of the shear strength. If the sample does not fail because of differences among the samples in the last shear stress level, then the increment of the shear stress ( $\Delta\sigma$ ) would be changed to 5% of the shear strength. A steady creep stage and the same duration of application of each stress level are required to conduct the multi-step loading tests. According to the preliminary tests, all creep tests performed on the samples with different roughness values and various normal stresses entered the steady creep stage within 24 h; each stage of the shear stress level is kept constant for approximately 72 h in our tests. The actual shear creep stresses and creep failure stresses in the multi-step creep tests are listed in Table 3. The test number is named with the number of Barton’s standard profile line and normal stress. The samples fail in the creep section in the tests of 1–2.17.1–6.52, 10–4.35, and 10–6.52, and fail in the loading section in the tests of 1–4.35 and 10–2.17.

To eliminate any effect of temperature and moisture fluctuation on either the sample or equipment, the temperature is controlled at  $20 \pm 1$  °C, and the relative humidity is maintained at  $50 \pm 2\%$  using a constant temperature humidistat.

**Table 3** Information of multi-step creep tests

JRC	Tests	Creep stress/MPa	Failure stress/MPa	Failure mode
JRC=1	1–2.17	0.88, 1.06, 1.23, 1.41, 1.584	1.70	Creep
	1–4.35	1.945, 2.334, 2.723, 3.112, 3.501, 3.7	3.91	Instantaneous
	1–6.52	2.35, 2.82, 3.29, 3.76, 4.23	4.70	Creep
	10–2.17	1.79, 2.15, 2.51, 2.86, 3.22	3.58	Instantaneous
JRC=19	10–4.35	3.13, 3.75, 4.38, 5.0, 5.63	6.28	Creep
	10–6.52	3.5, 4.2, 4.9, 5.6, 6.5, 7.0, 7.7	7.75	Creep

## Results and discussion

### Creep characteristics of discontinuities with different JRCs and normal stresses

#### Shear creep characteristics of rock discontinuities

The creep curves of the last stages in the tests that end in the creep section are plotted in Fig. 4. The creep rate is calculated using Eq. (1) based on the creep test results plotted in Fig. 4 (Wang et al. 2018):

$$v_D = \Delta D / \Delta t \tag{1}$$

where  $v_D$  is the creep rate,  $\Delta D$  the increment of creep deformation, and  $\Delta t$  the corresponding time.

The three stages, including transition creep stage, steady creep stage, and accelerating creep stage, can be observed in the last creep stage of the multi-step creep tests, as shown in

Fig. 4. The durations are random, and the regularity is difficult to observe because of differences among the samples and the complexity of influencing factors. For example, the steady creep stage lasted for approximately 72 h and thereafter entered the accelerating creep stage in test 1–4.35. In test 10–4.35, however, the creep stage only lasted for 40 s. As shown in Fig. 5, once the creep enters the accelerating creep stage, failure occurs in a shorter time. It is probably late to employ the engineering treatment to control the creep deformation once the creep enters the accelerating creep stage. The characteristics of the transition and steady creep stages therefore are also important for rock engineering and controlling creep in the first two stages.

In the steady creep stage, the curves do not appear to be linear, and the fluctuations can be observed in the tests, as shown in Fig. 4 (area A). The test results prove that the steady creep stage curve is not perfectly linear. In fact, the overall trend of the creep process exhibits deceleration, and the local fluctuation is caused by the fracture in the creep

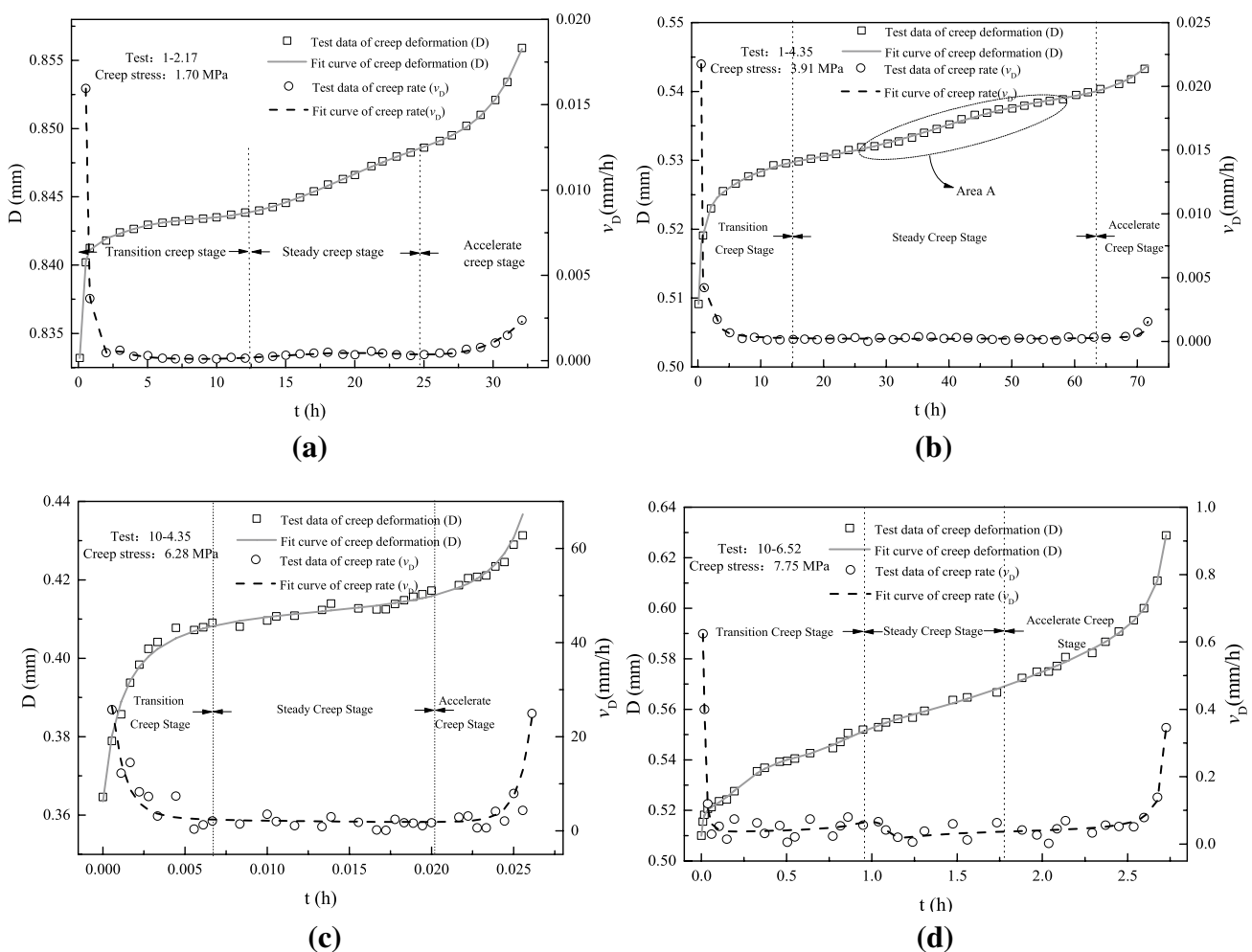
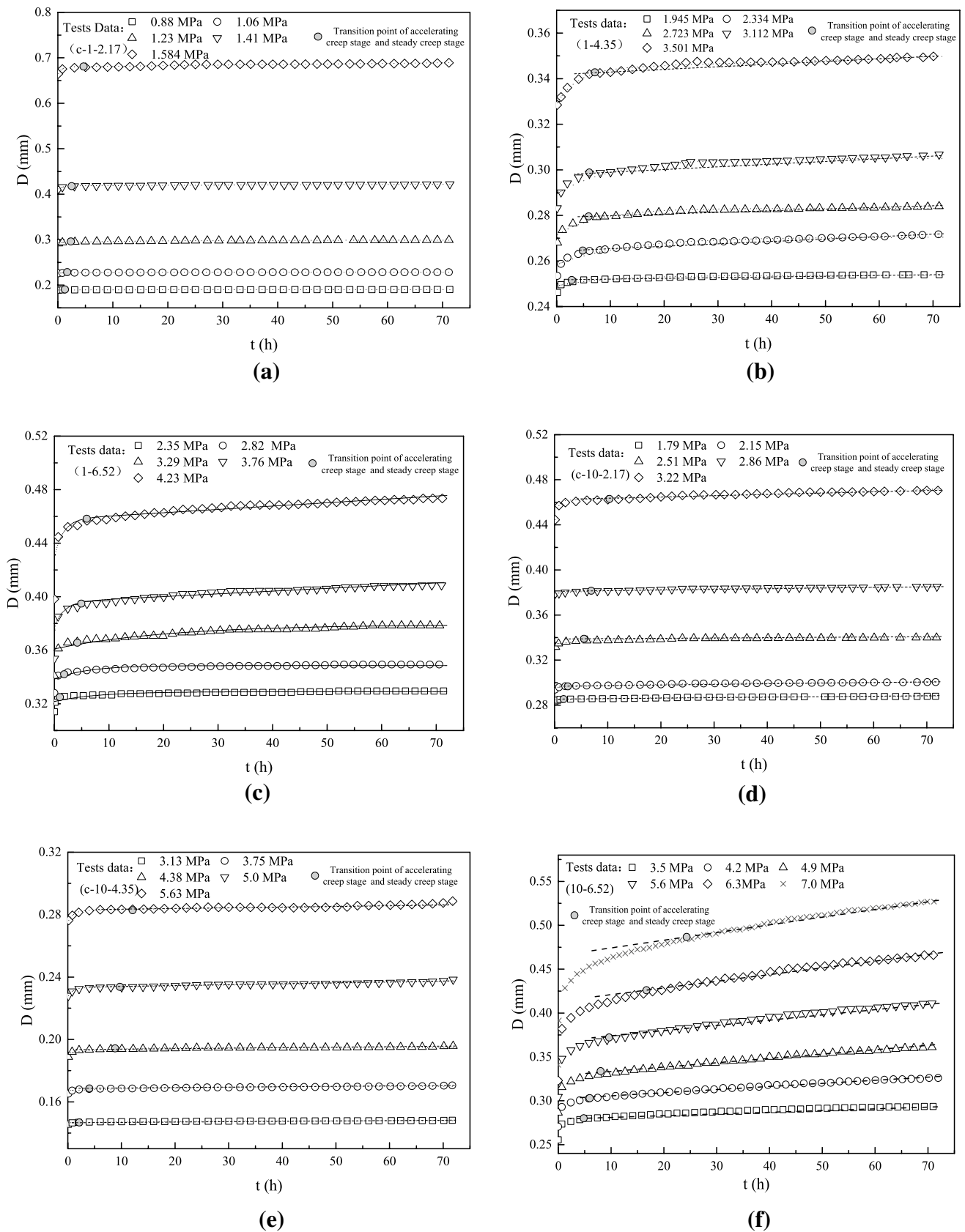


Fig. 4 Creep and creep rate curves of discontinuities with different JRCs and creep stresses



**Fig. 5** One-step loading creep curves and trend curves (the multi-stage creep tests' data were the organized data by the method recommend by Tan (1966) to obtain this figure. The transition point indicates the transition points from the transient creep stage to the steady creep stage)

process. As shown in Fig. 4b, the creep curves are nonlinear, and the creep rate first decreases and thereafter increases (area A). The increase in creep rate is caused by the sudden fracture, as indicated by a cracking sound during the tests. The force that prevents sliding decreases, and the creep rate accelerates. The creep rate decelerates, however, after a short acceleration period when shearing is prevented again. This phenomenon can easily be mistakenly regarded as the beginning of the accelerating creep stage.

The failure characteristics of the discontinuities are also influenced by different joint roughness coefficients (JRCs). As shown in Fig. 4, when JRC = 1, a longer period of time is necessary to reach a higher creep rate. When JRC = 19, however, the creep failure is intense, and the creep rate rapidly increases after entering the accelerating creep stage, which has a short duration. This indicates that the creep characteristics of rock discontinuity are closely related to the JRC. The larger the JRC, the larger the proportion of cutting asperity during the shear process, and more space for power storage to accelerate the creep rate is available. A higher creep stress provides more power. Normal stress is also one of the key factors that influence the creep failure mode of rock discontinuities. The shear mode also transforms into cutting asperity from friction as the normal stress increases, which corresponds to the increase in JRC. It has a mechanism similar to the one that influences the shear creep property.

**Characteristics and empirical constitutive model of transition and steady creep stages**

A method proposed by Tan (1966) and Tan and Kang (1980) based on the general Boltzmann superposition theorem is used for organizing the multi-step creep tests to obtain the one-step loading creep curves in each creep stress level. The creep curves under different creep stresses, which are lower than failure stress, are shown in Fig. 5. As soon as the creep stresses are applied, creep deformation develops at a high initial rate. The rate starts to fall thereafter decreases and tends to stabilize; the curves somewhat exhibit a linear trend. Fluctuations, which indicate that the curve of the steady creep stage is not strictly linear, are also observed. When the creep stress is high, a slope indicating that the creep rate of the aforementioned stage is large, is observed, and the slope decreases as the creep stress decreases.

The transition points for both the transition and steady creep stages can be observed according to the characteristics of creep curves, as shown in Fig. 5. The transition creep stage duration increases with increasing normal stress, JRC, and creep stress. When the normal stress or JRC is large, the sample has a better ability to store energy and a larger creep stress can provide more energy to drive creep.

The creep deformation is composed of creep and instantaneous deformations. The creep deformation at different stress ratios and normal stresses within 72 h based on the data from the general Boltzmann superposition theorem are shown in Fig. 6. The creep deformation proportion ( $D_c/D_T$ ) increases with increases in JRC, normal stress, and stress ratio ( $R$ ).

As shown in Fig. 7, the creep deformation develops at a high initial rate, immediately after the stresses are applied. It thereafter decreases and tends to stabilize at a relatively constant value, as expressed by

$$v_D = m_c t^{n_c} + v_c \tag{2}$$

where  $v_D$  is the creep rate,  $t$  is the creep time,  $v_c$  is the creep rate at the end of the steady creep rate, and  $m_c$  and  $n_c$  are the fitting parameters;  $n_c < 0$ .

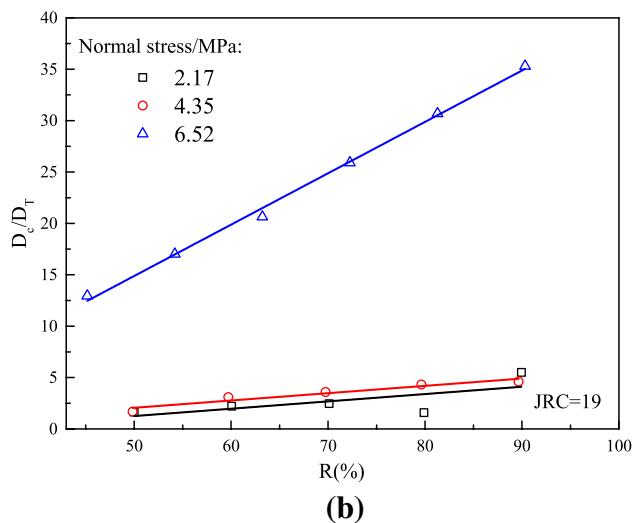
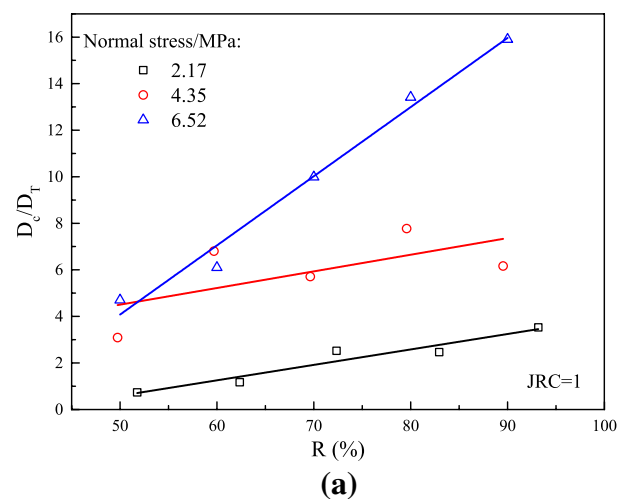


**Fig. 6** Composition of the creep deformation under different stress ratio and normal stress ( $D_c$  is creep deformation,  $D_T$  is the total deformation, and  $R$  is the ratio of creep stress and shear strength)

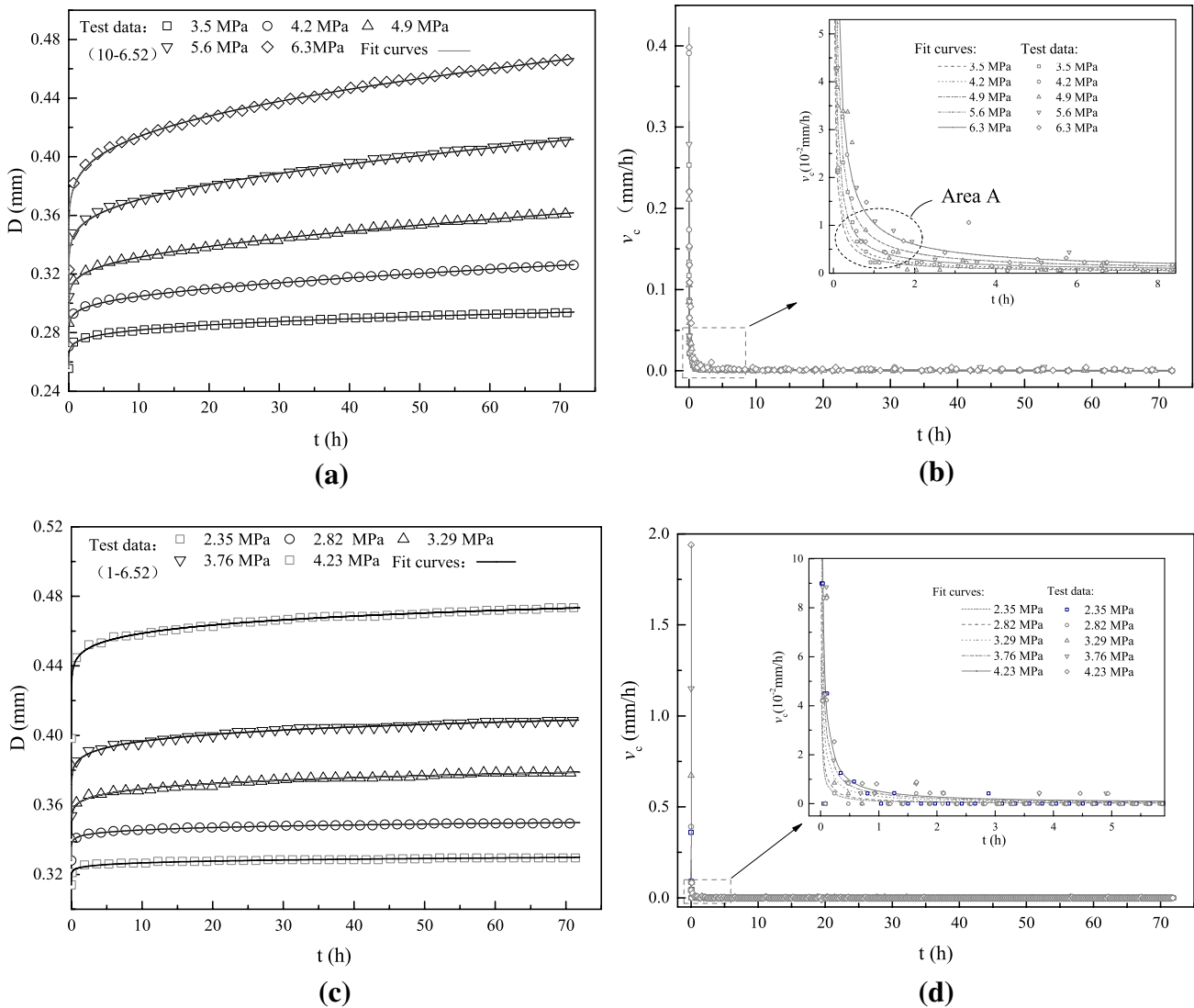


Fig. 7 Fit curves based on the empirical creep constitutive model

Equation (1) can be rewritten as follows.

$$\frac{dD}{dt} = m_c t^{n_c} + v_c \tag{3}$$

The integral can be obtained by Eqs. (2) and (3):

$$D = \frac{m_c}{(n_c + 1)} t^{n_c+1} + v_c t + D_i \tag{4}$$

where  $D_i$  is the integration constant, which is defined as the instantaneous deformation before the shear creep stage. In Eqs. (2) and (4), parameter  $n_c$  determines the decay rate of creep rate. As the absolute value of  $n_c$  increases, the decay rate increases, indicating that the creep rate rapidly tends to stabilize and control the creep duration. In Eq. (4), parameter

$m_c$  controls the total value of creep deformation, and  $v_c$  is the creep rate at the end of the steady creep stage.

The fitting results of Eq. (3) and test results are plotted in Fig. 8 and summarized in Table 4. This equation can be used to clearly describe the creep curves of both the transition and steady creep stages. Meanwhile, the creep rate characteristics can also be calculated using the fitting parameters of Eqs. (1) and (3).

As shown in Fig. 8a and c, parameter  $m_c$ , which represents the variation of creep deformation, increases with the creep stress, JRC, and normal stress. Parameter  $n_c$ , which determines the decay rate of creep rate and duration of creep, decreases at first and thereafter increases with the creep stress, as shown in Fig. 8b and d. This indicates that the creep duration increase initially followed by a decrease. Its variation characteristics are



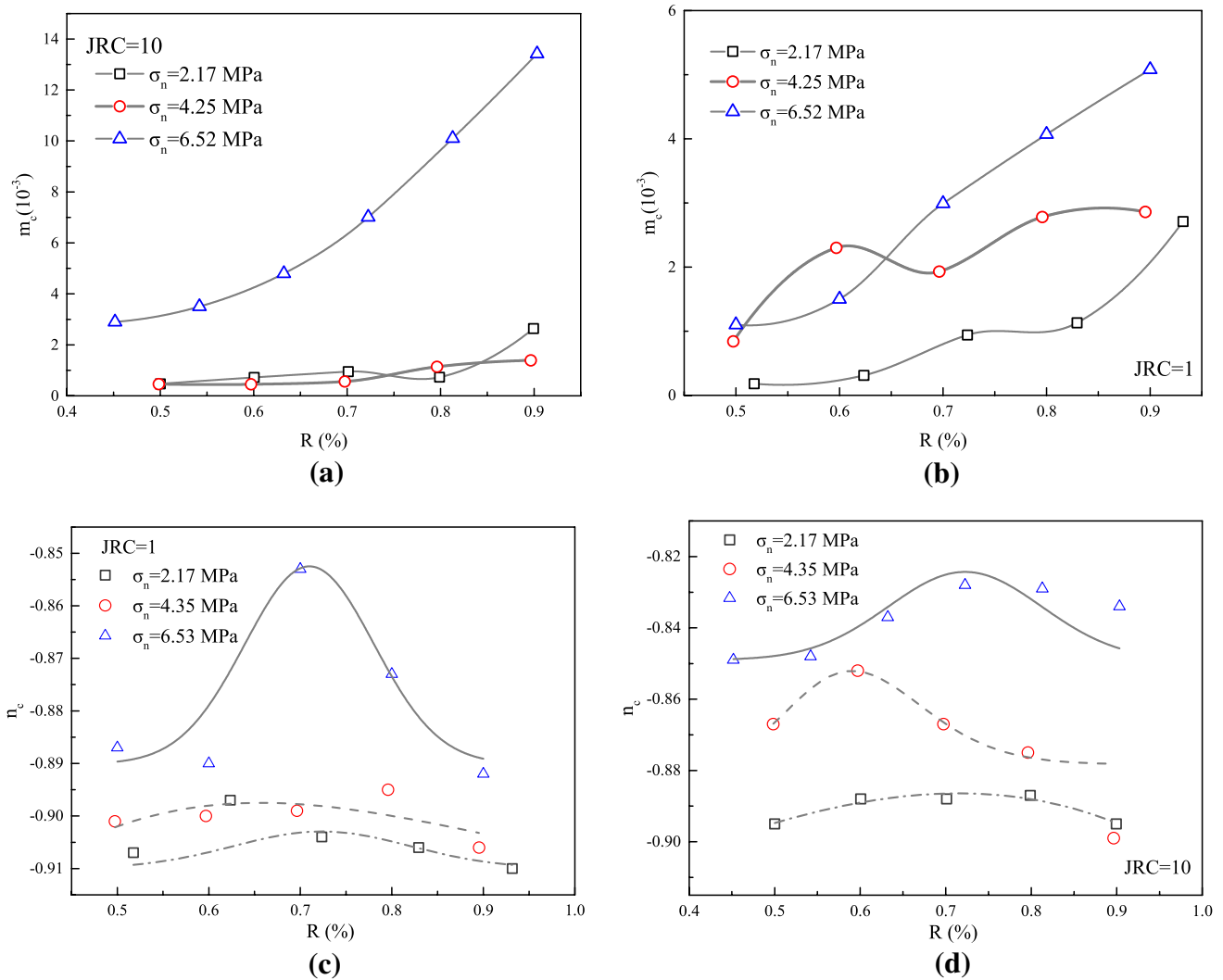


**Fig. 8** Relationships between fitting parameters ( $m_c$ ,  $n_c$ ) and stress ratio ( $R$  creep stress/shear strength)

**Table 4** Parameters of JRCW model (normal stress: 6.52 MPa)

JRC	$v_s$ /MPa/min	$\varphi_b/^\circ$	$m$	$D_f$ /mm	JRCr	$D_f$ /mm	$\tau_{ps}$
19	0.5	32.38	0.162	0.56	1.2	0.59	1.52

similar to those of the shear stiffness during the shear process (Wang et al. 2020). Parameter  $n_c$  increases as the JRC and normal stress, which means that the decay rate of the creep rate slows down, and the creep requires more time to stabilize.

**Prediction of starting point of accelerating creep stage and creep failure**

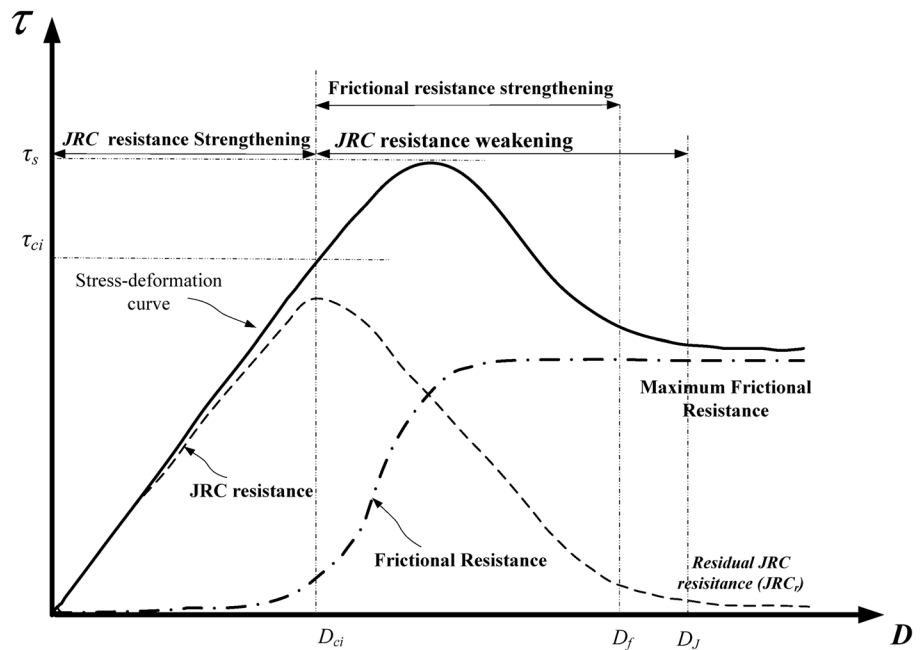
**JRCW model**

The shear strength is composed of the JRC and frictional resistance, which are not mobilized simultaneously (Wang

et al. 2020). The direct shear test is a process of the JRC resistance weakening and frictional resistance strengthening because of the crack development in the asperities and climbing asperities in the shearing process. The mobilization of strength components are shown in Fig. 9.

A model named JRC resistance weakening and frictional resistance strengthening model (JRCW) was proposed by Wang et al. (2020) according to the mobilization of strength components. The JRCW model can be written as

**Fig. 9** Mobilization of strength components (Wang et al. 2020) ( $D_{ci}$  peak mobilization of JRC resistance,  $D_j$  residual JRC resistance,  $D_f$  peak mobilization of frictional resistance,  $JRC_r$  residual JRC)



$$\tau = \begin{cases} k_a D, \tau \leq \tau_{ci} \\ f(mJRC, D_p) + f(\sigma_n \tan \varphi_b, D_p), \tau > \tau_{ci} \end{cases} \quad (5)$$

where  $k_a$  is the shear stiffness prior to the initial crack occurrence, and

$$f(mJRC, D_p) = m(JRC - JRC_r)e^{-\xi} + mJRC_r, \xi = (D_p/D_j)^2 \quad (6)$$

$$f(\sigma_n \tan \varphi_b, D_p) = \begin{cases} \left(2 \frac{\sqrt{D_p D_f}}{D_p + D_f}\right) \sigma_n \tan \varphi_b + \tau_{\mu s}, & D_p \leq D_f \\ \sigma_n \tan \varphi_b + \tau_{\mu s}, & D_p > D_f \end{cases} \quad (7)$$

where  $m$  is the JRC exertion coefficient,  $D_p$  the equivalent plastic deformation related to both plastic deformation and crack growth,  $\sigma_n$  the normal stress,  $\varphi_b$  the friction angle when  $JRC = 0$ ,  $D_f$  the deformation limits of the peak mobilization of the frictional resistance,  $JRC_r$  the residual JRC,  $\xi$  the parameter related to crack growth and plastic deformation, and  $\tau_{\mu s}$  the frictional resistance prior to the occurrence of initial crack (Wang et al. 2020).

**JRC resistance weakening–frictional resistance compensation creep model (JRCWC model)**

In the creep tests, acoustic emissions are monitored (Wang et al. 2015). It is found that the creep deformation is closely related to crack development. When the creep stress is kept constant, the continuous energy therefore results in the occurrence and development of cracks. The phenomena can

also lead to the JRC resistance weakening, which has the same mechanism as the resistance mobilization in the shear process. Meanwhile, to keep the creep stress constant, the frictional resistance must be mobilized to compensate for the loss of the JRC resistance. If the frictional resistance cannot compensate for it, the creep rate would accelerate, and the tests enter the accelerating creep stage.

According to the shear creep mechanism above, the deterioration of the JRC resistance can be described using Eq. (8) as follows:

$$|\Delta f(mJRC, D_p)| = f(mJRC, D_{ps}) - f(mJRC, D_p) \quad (8)$$

where  $|\Delta f(mJRC, D_p)|$  is the loss of JRC resistance,  $f(mJRC, D_{ps})$  is the JRC resistance in the instantaneous deformation section,  $D_{ps}$  is the equivalent plastic deformation before creep, and  $f(mJRC, D_p)$  is the JRC resistance when the equivalent plastic deformation is  $D_p$ :  $D_p > D_{ps}$ .

According to the results reported by Wang et al. (2020), the JRCW resistance varies with  $D_p$ , the shape of the JRC resistance curve is controlled by  $D_j$ , which is not related to shear rate. The frictional resistance, however, also varies with  $D_p$ , and the shape of the frictional resistance curve is controlled by  $D_f$ , which is closely related with shear rate, especially the sliding rate of the sample. In the creep tests, the JRC resistance decreases with the increase in  $D_p$ , and the creep rate would increase because the load is larger than the resistance. Frictional resistance is mobilized with the increase in creep rate, and it will be adjusted as the variation of creep rates keeps the creep stress constant. To maintain the balance between loading and resistance, the frictional

resistance must therefore compensate for the loss of the JRC resistance. It can be described as follows:

$$|\Delta f(mJRC, D_p)| = |\Delta f(\sigma_n \tan \varphi_b, D_p)| \tag{9}$$

where  $|\Delta f(mJRC, D_p)|$  is the loss of JRC resistance and  $|\Delta f(\sigma_n \tan \varphi_b, D_p)|$  the compensation resistance that comes from frictional resistance. The loss of the JRC resistance can be written as

$$|\Delta f(mJRC, D_p)| = f(mJRC, D_{ps}) - f(mJRC, D_p) \tag{10}$$

where  $f(mJRC, D_{ps})$  is the JRC resistance at the end of the loading section. It is caused by the instantaneous plastic deformation;  $f(mJRC, D_p)$  is been given in Eq. (6).

The compensation curve can be described as follows:

$$f_c(\sigma_n \tan \varphi_b, D_p) = f(\sigma_n \tan \varphi_b, D_{ps}) + |\Delta f(mJRC, D_p)| \tag{11}$$

where  $f(\sigma_n \tan \varphi_b, D_{ps})$  is the mobilization of the frictional resistance at the end of the loading section.

The combination of Eqs. (10) and (11) with the JRCW model, named as JRCWC model, can be used to describe the process of the JRC resistance weakening and frictional compensation. It can also predict the starting point of the accelerating creep stage.

**Prediction of starting point of accelerating creep stage using JRCWC model**

When the creep stress is large, the occurrence and development of cracks cause the continuous decrease in JRC resistance. The frictional resistance can compensate for the loss of JRC resistance within a certain time. Once the frictional resistance reaches the maximum, the cracks continue to develop, the loss of JRC resistance cannot be compensated by frictional resistance, the loading stress begins to become larger than the sum of JRC resistance and frictional resistance, the creep rate begins to accelerate, and the accelerating creep stage would start. The combination of the empirical transition creep model and steady creep model can be employed to predict the creep failure time.

Consider test c-10-6.52 as example. The parameters of JRCW model could be determined based on the shear test data. As summarized in Table 4 and shown in Fig. 10, the shear test is conducted on the sample with JRC = 19; the shear rate ( $v_s$ ) is 0.5 MPa/min. Parameter  $\varphi_b$  is obtained by shear tests when JRC = 0. Parameter  $m$  is obtained by the initial crack strength (Wang 2020), and parameters  $D_j$ ,  $JRC_r$ ,  $D_f$ , and  $\tau_{\mu s}$  are determined by simulating the shear test curve. The calculated curve and test curve are plotted in Fig. 10.

The JRC resistance and corresponding compensation curve under lower creep stresses are shown in Fig. 11. In the coordinate system of shear stress ( $\tau$ ) and equivalent plastic deformation ( $D_p$ ), the curves of the creep section are horizontal lines. As shown in Fig. 11, frictional resistance could always compensate for the JRC resistance loss because the maximum frictional resistance is larger than the maximum JRC resistance loss. Once the mobilized frictional resistance is sufficiently large that the rest of the creep stresses (creep stress-frictional resistance) cannot result in cracks and plastic deformation, the JRC resistance ceases to decrease. By this time, creep stops as well.

The JRC resistance curve and compensation curve when the creep stress is large are shown in Fig. 12. Parameter  $D_f$  also varies with the creep rate and compensates for the loss of JRC resistance. When the compensation resistance exceeds the maximum frictional resistance, however, the creep rate begins to increase, and the creep enters the accelerating creep stage. At this critical state, the compensation strength is equal to the maximum frictional resistance. The above analysis can thus be described using Eqs. (7) and (11) as follows.

$$f_c(\sigma_n \tan \varphi_b, D_p) = f(\sigma_n \tan \varphi_b, D_{ps}) + |\Delta f(mJRC, D_p)| = \sigma_n \tan \varphi_b + \tau_{\mu s} \tag{12}$$

Equation (12) could be used to predict the equivalent plastic deformation ( $D_p$ ). When combined with the empirical creep constructive model (Eq. (3)), the time upon entering the accelerating creep stage can be calculated. When the creep stress is 6.3 MPa, the equivalent plastic deformation ( $D_p$ ) is 0.77 mm, and the creep deformation is 0.742 mm, as calculated by  $D_p - D_i$ . The creep enters the accelerating creep stage at 1852 h. When the creep

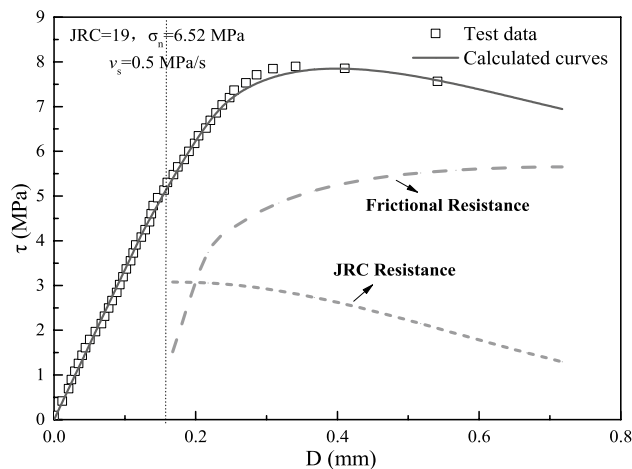


Fig. 10 Shear test curve and calculated curve (10–6.52)

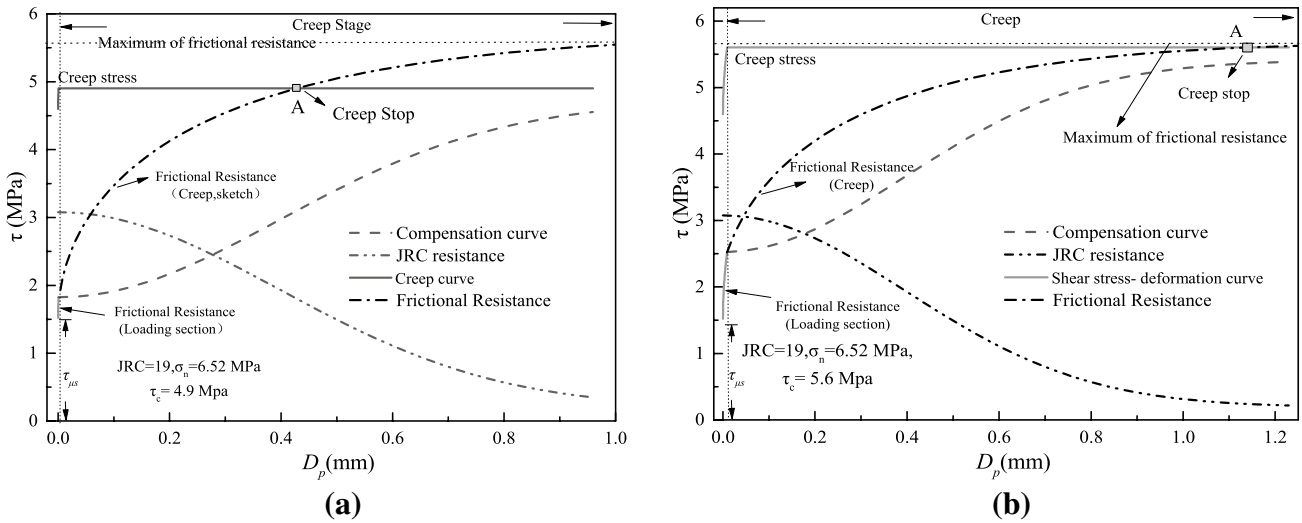


Fig. 11 JRC resistance loss and frictional resistance compensation in creep tests

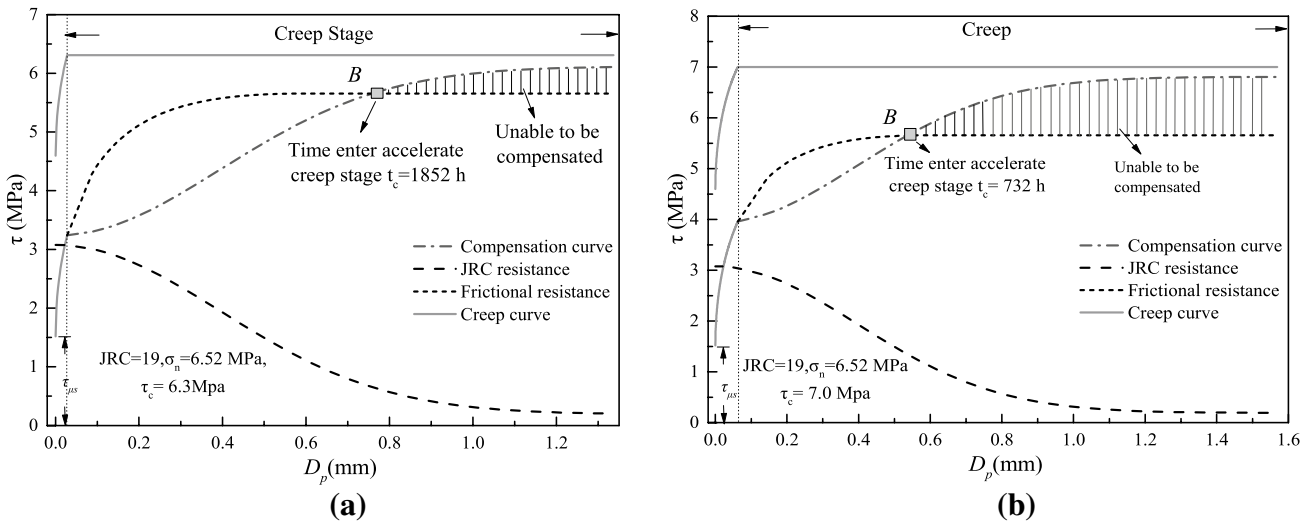


Fig. 12 JRC resistance loss and frictional resistance compensation in creep tests (failure)

stress is 7.0 MPa, the equivalent plastic deformation ( $D_p$ ) is 0.54 mm, and the creep deformation is 0.4772 mm. The creep enters the accelerating creep stage at 732 h (Point B).

**Method for determining long-term strength based on deformation at starting point of accelerating creep stage**

The deformation of the starting point of the accelerating creep stage can be calculated according to Eq. (12) and Fig. 13 (this figure shows a reverse S-shaped curve). When the creep stress approaches the shear strength, an equivalent plastic deformation is necessary to enter the accelerating creep stage. This deformation rapidly decreases as the creep

stress increases. Stage I is presented in Fig. 13. In stage II, an approximately linear relationship can be observed in the range 7.75–6.5 MPa. The creep deformation, which ensures that the creep enters the accelerating creep stage, has a linear relationship with the creep stress. It corresponds to the stabilized crack development in the shear process. When the creep stress is less than 6.5 MPa, an increasing equivalent plastic deformation would be necessary to enter the accelerating creep stage. It should be noted that the deformation in Fig. 13 is a one-step loading creep test; hence, the creep deformation before the accelerating creep stage is larger than that in the last stage of the multi-step creep tests in test 10–6.52.

The curve approaches the asymptotic line ( $\tau_c = 5.8$  MPa), which means that an infinite deformation is necessary to

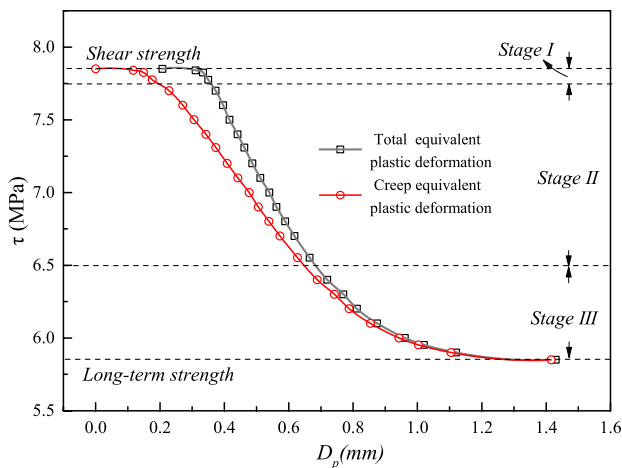


**Fig. 13** Relationships between equivalent plastic deformation and shear creep stress at the starting point of accelerating creep stage (total equivalent plastic deformation is the equivalent plastic deformation from initial crack to starting point of accelerating creep stage, creep equivalent plastic deformation is creep deformation before starting point of accelerating creep stage)

enter the accelerating creep stage. Simply put, when the creep stress is 5.8 MPa, only two stages can be observed in the creep tests. Once the sample is stressed beyond 5.8 MPa, the creep would enter the accelerating creep stage, and failure can be observed. This creep stress is the maximum stress that can keep the sample stable for a long duration. The definition of the threshold stress corresponds to the long-term strength; hence, the stress of asymptotic line can be regarded as the long-term strength.

## Conclusions

The shear creep characteristics of rock discontinuity are investigated, and the time upon which creep enters the accelerating creep stage is predicted. A series of multi-step creep tests are performed. Three stages can be observed, and the creep characteristics are investigated in detail. The empirical creep model that is used to describe both transition and steady creep stages is established. The shear creep mechanism of rock discontinuity is also explained using the JRC resistance weakening–frictional resistance compensation creep model. A method for determining the starting point, time, and deformation of the accelerating creep stage is proposed based on the JRCWC model and empirical creep model. The following conclusions are drawn:

1. The creep of rock discontinuity includes transition creep stage, steady creep stage, and accelerating creep stage. The creep curves that exhibit distinct nonlinear and local fluctuations caused by cracking can be observed from

the creep curve. The overall trend of the steady creep process is deceleration, and the curves of this stage are not strictly linear.

2. Creep characteristics are significantly influenced by creep stress, joint roughness coefficients (JRCs), and normal stress. The ratio of creep deformation to total deformation increases with the increases in creep stress, JRC, and normal stress. The creep failure characteristics and mode of discontinuities are also influenced by the foregoing. The failure would be more intense with increases in joint roughness and normal stress because the rock discontinuity with a larger JRC has a better energy storage ability.
3. The creep process can be described as involving the JRC resistance weakening and frictional resistance compensation. The mechanism of the creep entering the accelerating creep stage is that the frictional resistance cannot compensate for the loss of JRC resistance.
4. With the combination of the empirical creep model and JRCWC model that is used to describe the process of JRC resistance weakening and frictional resistance compensation during the creep test, the starting point of the accelerating creep stage can be predicted. The long-term strength can be calculated based on the relationship between the starting point deformation of the accelerating creep stage and creep stress.

**Acknowledgements** This work is financially supported by Open research fund of Key Laboratory of Geotechnical and Underground Engineering, Ministry of Education, Tongji University (Grant No. KLE-TJGE-B1903), and National Natural Science Foundation of China (Grant Nos. 51908288, 51809137).

## References

- Araki E, Saffer DM, Kopf AJ, Wallace LM, Kimura T, Machida Y, Ide S, Davis E, IODP Expedition 365 shipboard scientists (2017) Recurring and triggered slow-slip events near the trench at the Nankai Trough subduction megathrust. *Science* 356(6343):1157–1160
- Asanov VA, Pan'kov IL (2004) Deformation of salt rock joints in time. *J Min Sci* 40(4):355–359
- Brantut N, Baud P, Heap MJ, Meredith PG (2012) Micromechanics of brittle creep in rocks. *J Geophys Res* 117(B8):1133–1172
- Brantut N, Heap MJ, Meredith PG, Baud P (2013) Time-dependent cracking and brittle creep in crustal rocks: a review. *J Struct Geol* 52(5):17–43
- Barton N (1978) Suggested methods for the quantitative description of discontinuities in rock masses. *Int J Rock Mech Mining Sci Geomech Abstr* 15(06):319–368
- Boyd E, Bouvard A, Pellet F (2002) Back analysis of time-dependent behaviour of a test gallery in claystone. *Tunn Undergr Space Technol* 17(4):415–424
- Christensen RM (1982) *Theory of viscoelasticity*. Academic Press, New York

- Drescher K, Handley MF (2003) Aspects of time-dependent deformation in hard rock at great depth. *J South Afr Inst Min Metall* 103(5):325–335
- Einstein HH, Veneziano D, Baecher GB, O'Reilly KJ (1983) The effect of discontinuity persistence on rock slope stability. *Int J Rock Mech Mining Sci Geomech Abstr* 20(05):227–236
- He ZL, Zhu ZD, Li ZJ (2014) Study of nonlinear creep damage model of marble with structural plane. *Sci Technol Eng* 14(32):68–72
- Heap MJ, Baud P, Meredith PG, Bell AF, Main IG (2009) Time-dependent brittle creep in Darley Dale sandstone. *J Geophys Res* 114(B7):4288–4309
- Kemeny J (2003) The time-dependent reduction of sliding cohesion due to rock bridges along discontinuities: a fracture mechanics approach. *Rock Mech Rock Eng* 36(1):27–38
- Kemeny J (2005) Time-dependent drift degradation due to the progressive failure of rock bridges along discontinuities. *Int J Rock Mech Min Sci* 42(1):35–46
- Mulchrone KF, Mukherjee S (2015) Shear senses and viscous dissipation of layered ductile simple shear zones. *Pure Appl Geophys* 172(10):2635–2642
- Oppikofer T, Jaboyedoff M, Blikra L, Derron MH, Metzger R (2009) Characterization and monitoring of the Åknes rockslide using terrestrial laser scanning. *Nat Hazards Earth Syst Sci* 9(3):1003–1019
- Patton F D (1966). Multiple modes of shear failure in rock. 1st ISRM Congress. *Int Soc Rock Mech Rock Eng*
- Phienweij N, Thakur PK, Cording EJ (2007) Time-dependent response of tunnels considering creep effect. *Int J Geomech* 7(4):296–306
- Potyondy DO, Cundall PA (2004) A bonded-particle model for rock. *Int J Rock Mech Min Sci* 41(8):1329–1364
- Potyondy DO (2007) Simulating stress corrosion with a bonded-particle model for rock. *Int J Rock Mech Min Sci* 44(5):677–691
- Singh DP (1975) A study of creep of rocks. *Int J Rock Mech Min Sci* 12:271–276
- Sakurai S (1978) Approximate time-dependent analysis of tunnel support structure considering progress of tunnel face. *Int J Numer Anal Meth Geomech* 2(2):159–175
- Tan TK (1966) Determination of the Rheological Parameters and the Hardening Coefficients of Clays Rheology and Soil Mechanics. Springer, Berlin Heidelberg, pp 256–272
- Tan TK, Kang WF (1980) Locked in stresses, creep and dilatancy of rocks, and constitutive equations. *Rock Mech Rock Eng* 13(1):5–22
- Ulusay R (2015) ISRM suggested methods for rock characterization, testing and monitoring: 2007–2014. Springer, New York
- Wang YX, Wang JA, Tang J (2015) Acoustic emission characteristics of fractured rocks during creep shear. *Chin J Rock Mech Eng* 34(S1):2948–2958
- Wang Z, Shen MR, Ding WQ, Jang BA, Zhang QZ (2018) Time-dependent behavior of rough discontinuities under shearing conditions. *J Geophys Eng* 15(1):51
- Wang Z, Shen MR, Tian GH, Zhang QZ (2017) Time-dependent strength of rock mass discontinuity with different values of JRC. *Chin J Rock Mech Eng* 36:3287–3296
- Wang Z, Gu LL, Shen MR, Zhang F, Zhang GK, Deng SX (2020) Influence of shear rate on the shear strength of discontinuities with different joint roughness coefficients. *Geotech Test J* 43(3):20180291
- Xu T, Xu Q, Tang CA, Ranjith PG (2013) The evolution of rock failure with discontinuities due to shear creep. *Acta Geotech* 8(6):567–581
- Zhang F, Xiong YL, Itani Y (2019) Thermo-elasto-viscoplastic mechanical behavior of manmade rock and its numerical modeling. *Underground Space* 4(2):121–132
- Zhang QZ, Shen MR, Wen Z (2011) Investigation on mechanical behavior of a rock plane using rheological tests. *J Mater Civ Eng* 23:1220–1226
- Zhu ZD, Li ZJ, Zhu ML, Wang Q (2009) Shear rheological experiment on rock mass discontinuities and back analysis of model parameters. *Rock Soil Mech* 30:99–104